INTERFACE

royalsocietypublishing.org/journal/rsif

Research

Cite this article: Leventhal GE, Ackermann M, Schiessl KT. 2019 Why microbes secrete molecules to modify their environment: the case of iron-chelating siderophores. *J. R. Soc. Interface* **16**: 20180674.
http://dx.doi.org/10.1098/rsif.2018.0674

Received: 6 September 2018
Accepted: 30 November 2018

Subject Category:
Life Sciences–Physics interface

Subject Areas:
systems biology, evolution, environmental science

Keywords:
siderophores, secretion, public goods, iron uptake, diffusion

Authors for correspondence:
Gabriel E. Leventhal
e-mail: gaberoo@mit.edu
Konstanze T. Schiessl
e-mail: konstanze.schiessl@gmail.com

Electronic supplementary material is available online at https://dx.doi.org/10.6084/m9.figshare.c.4329440.

THE ROYAL SOCIETY PUBLISHING

Why microbes secrete molecules to modify their environment: the case of iron-chelating siderophores

Gabriel E. Leventhal[1,2], Martin Ackermann[3,4] and Konstanze T. Schiessl[3,4,5]

[1]Department of Civil and Environmental Engineering, Massachusetts Institute of Technology (MIT), Cambridge, MA, USA
[2]Institute of Integrative Biology, Swiss Federal Institute of Technology Zurich (ETH Zurich), Zurich, Switzerland
[3]Institute of Biogeochemistry and Pollutant Dynamics, Swiss Federal Institute of Technology Zurich (ETH Zurich), Zurich, Switzerland
[4]Department of Environmental Microbiology, Swiss Federal Institute of Aquatic Science and Technology (Eawag), Dübendorf, Switzerland
[5]Department of Biological Sciences, Columbia University, New York, NY, USA

GEL, 0000-0002-4463-166X; MA, 0000-0003-0087-4819; KTS, 0000-0002-1053-5610

Many microorganisms secrete molecules that interact with resources outside of the cell. This includes, for example, enzymes that degrade polymers like chitin, and chelators that bind trace metals like iron. In contrast to direct uptake via the cell surface, such release strategies entail the risk of losing the secreted molecules to environmental sinks, including 'cheating' genotypes. Nevertheless, such secretion strategies are widespread, even in the well-mixed marine environment. Here, we investigate the benefits of a release strategy whose efficiency has frequently been questioned: iron uptake in the ocean by secretion of iron chelators called siderophores. We asked the question whether the release itself is essential for the function of siderophores, which could explain why this risky release strategy is widespread. We developed a reaction–diffusion model to determine the impact of siderophore release on iron uptake from the predominant iron sources in marine environments, colloidal or particulate iron, formed due to poor iron solubility. We found that release of siderophores is essential to accelerate iron uptake, as secreted siderophores transform slowly diffusing large iron particles to small, quickly diffusing iron–siderophore complexes. In addition, we found that cells can synergistically share their siderophores, depending on their distance and the size of the iron sources. Our study helps understand why release of siderophores is so widespread: even though a large fraction of siderophores is lost, the solubilization of iron through secreted siderophores can efficiently increase iron uptake, especially if siderophores are produced cooperatively by several cells. Overall, resource uptake mediated via release of molecules transforming their substrate could be essential to overcome diffusion limitation specifically in the cases of large, aggregated resources. In addition, we find that including the reaction of the released molecule with the substrate can impact the result of cooperative and competitive interactions, making our model also relevant for release-based uptake of other substrates.

1. Introduction

Bacteria secrete massive amounts of metabolites and proteins into the environment, many of them involved in nutrient uptake. Examples include secreted exoproteases, chitinases or trace metal chelators like siderophores (chelating iron) or methanobactin (chelating copper). The secreted molecules transform their substrate (by degradation or chelation), which is then taken up by the bacterial cell. Release-based nutrient uptake strategies have been investigated as examples for cooperative behaviour in bacteria as well as probed for their stability to the 'public goods dilemma' [1,2], as the benefits gained by released metabolites, the transformed substrates, become available to cells not contributing to

production. In addition, especially in well-mixed environments, generated substrates might be lost to the environment and not diffuse back to the producing cell. Nevertheless, release-based uptake strategies are widespread. We were thus interested in understanding what benefits are specifically generated by release, and investigated this in a prominent example: the uptake of iron by siderophores in the well-mixed ocean environment.

Bacterial metabolism requires iron and hence the limited availability of iron in many environments restrains bacterial growth and reproduction [3–6]. One common cause of iron limitation is simply low concentrations of iron such as in ocean surface waters [7,8]. In addition, other factors further limit the bioavailability of iron in seawater. First, as in all oxic, pH-neutral environments, iron is only poorly soluble [9,10]. Hence, iron mostly occurs in particles of different sizes, which are often operationally defined in the marine environment as soluble (less than 0.02 μm), colloidal (0.02–0.4μm) and particulate (greater than 0.4 μm) [7,8,11,12]. Second, the soluble and colloidal fractions of iron are largely complexed by organic ligands and are thus only available for uptake by bacteria by expressing the cognate transporter or by disassociating the iron from the ligand [13]. While the effects of the presence of organic ligands on bacterial iron uptake has received considerable attention [14,15], the impact of colloidal and particulate iron on bacterial growth is still poorly understood [8,12]. Nevertheless, these larger types of iron sources are prevalent throughout the ocean [11,16–18] and can constitute up to 85% of the accessible iron pools [19].

Many microbes have developed strategies to increase iron bioavailability. One particularly widespread and well studied such strategy is siderophore secretion [20]. Siderophores are chelators that bacteria release into the environment to bind iron. The resulting iron–siderophore complexes can then be taken up by the bacteria. An important consequence of secretion is that a cell might not recapture and hence benefit from the siderophores it produced itself, due to random diffusion of the siderophore molecules. In dilute, well-mixed environments, the probability of recapturing a siderophore once it is secreted is low, and a solitary bacterium thus has to produce a large number of siderophores in order to achieve sufficient uptake of iron [21]. Hence, siderophore secretion has been viewed as a strategy poorly adapted to the marine environment [22]. Also, released siderophores can be taken up by strains that do not contribute to siderophore production if these express the cognate receptor [23,24]. This can lead to a public goods dilemma, where non-producing genotypes can displace bacteria that produce siderophores [25]. Thus, it is not obvious why the release of siderophores is efficient, especially in the marine environment.

Different mechanisms have been suggested that could mitigate the negative effects of release. Amphiphilic siderophores—containing both a fatty-acid tail and a hydrophilic head group—can constitute a considerable fraction of siderophores isolated from seawater samples [26]. Such siderophores might stay attached to the cell membrane of the producing cell thanks to their fatty-acid side chain [27–29] or might be more easily retained due to lower diffusivity [30]. Furthermore, inorganic ferric iron can be acquired directly using ATP-binding cassette transporters that are frequently detected in marine bacterial genomes [31,32]. In addition, surface-associated reductases allow uptake from particulate iron [33–35], outer membrane receptors mediate uptake of iron bound to exogenous chelators like heme or transferrin [36], and ferric citrate can be taken up via transporters or porins [37].

Despite the existence of such alternative mechanisms that avoid the risk of siderophore loss, siderophore secretion is widespread in bacteria [38], and has been described as key for iron uptake in environments with low iron availability [39]. This suggests that the release itself of siderophores might be directly beneficial for their function. However, it is less clear what the possible benefits might be. Here, we were specifically interested in comparing the efficiency of bacterial iron uptake based on release of siderophores to a strategy avoiding release (e.g. mediated by membrane-associated amphiphilic siderophores). We developed a mathematical model to quantify the benefits of siderophore release in marine surface waters. We focus on the marine environment because of the wealth of data on iron distributions and because the efficiency of siderophore secretion in the ocean has been questioned before [21]. In contrast to this previous model, we take larger-sized particulate and colloidal iron as potential iron sources into account. Note that while the precise operational distinction between dissolved and colloidal iron has since shifted slightly, we here explicitly model the size-dependent mass transport properties of iron particles. Previous models (like the free ion activity model) assumed diffusion of iron sources to be instantaneous compared to uptake across the cytoplasmic membrane [40]. By contrast, we hypothesize that in order to understand benefits that lie in the *release* of siderophores, diffusion limitation is a key factor and needs to be taken into account, in line with previously voiced criticism for neglecting the role of diffusion in iron uptake [40–42].

We hypothesize that siderophores 'scavenge' iron from larger-sized iron sources that diffuse more slowly than soluble iron or iron–siderophore chelates, thus providing benefits beyond just releasing soluble iron from organic ligands [21]. Using a mathematical model for the diffusion and bacterial uptake of iron, we find that release of siderophores can be of key importance to overcome iron limitation in conditions where mass transfer limits iron uptake. Under these conditions, where iron uptake is slowed down due to diffusion limitation of large iron particles, only secreted siderophores, i.e. siderophores released from the cell, can accelerate iron uptake. Furthermore, we find that the production of siderophores in groups of cells increases the efficiency of siderophore-based iron uptake, concurrent with previous literature [21]. The secretion of siderophores by multiple cells acts synergistically, as long as the cells are sufficiently far apart. These results suggest that the act of 'secreting' siderophores itself has innate benefits to bacterial growth and could explain why even single marine cells engage in siderophore release.

2. Results

2.1. Modelling iron particle size as the number of contained iron ions

We investigate iron uptake with a focus on the effect of low iron solubility on diffusion limitation. A key consequence of low iron solubility is that the majority of iron is present in aggregates such as colloidal (less than 0.4 μm) and particulate iron (greater than 0.4 μm) [7,11,19]. The diffusion speed of a particle will depend on its size, and hence by modelling

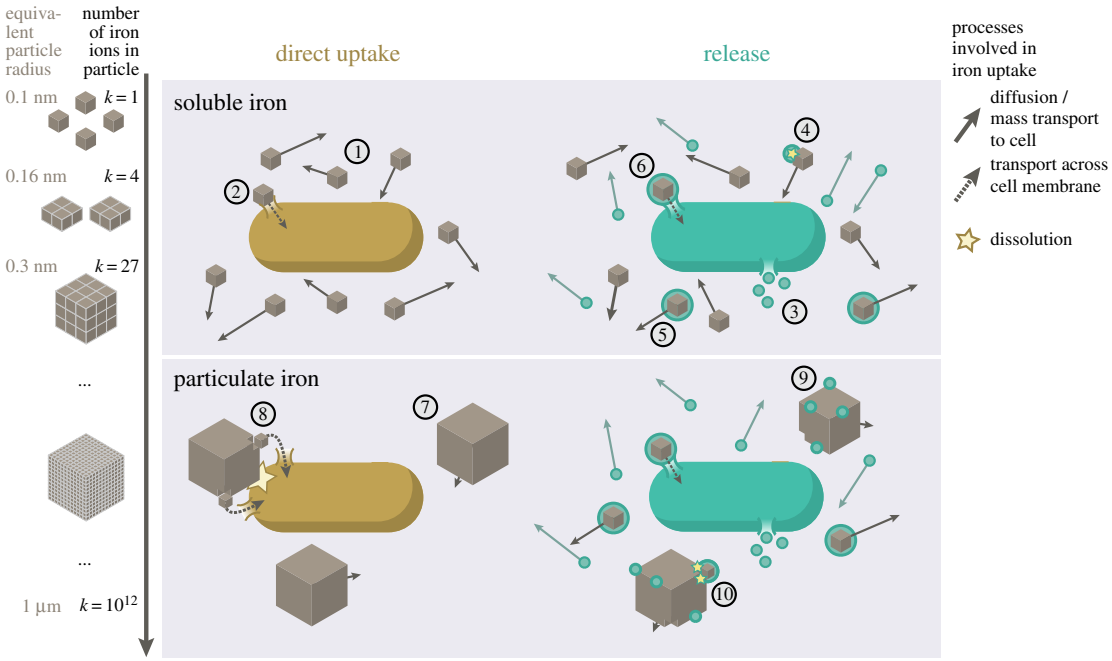

Figure 1. Modelling the direct and siderophore-mediated uptake of soluble and particulate iron. This figure illustrates iron uptake in the two extreme cases of very strong iron aggregation or complete solubility. When iron is fully soluble and freely diffusing (1), non-secreting (yellow) cells must take up iron ions directly (2). Secreter cells (green) release siderophores (3) that themselves diffuse freely and encounter and bind soluble iron (4). The resulting iron–siderophore complexes also diffuse freely (5), and are subsequently taken up by the cell (6). In the presence of large particulate iron sources (7), non-secreter cells must first encounter a particle before extracting individual iron ions to take up (8) using surface-bound ligands or reductases. This activity is limited by the number of iron particles a cell encounters and can 'hold on' to, as well as the rate at which it actively dissolves the particulate iron. Siderophores bind to the surface of the particle (9), and subsequently disassociate from it as an iron–siderophore complex (10). This occurs at a distance from the cell, therefore alleviating the restrictions on how many particles can be actively dissolved simultaneously. We want to point out that in our model, iron sources are modelled as spheres, not cubes.

iron particles of varying size, we can capture the diffusion of such aggregated iron particles in marine environments.

We assume that the iron particles are spherical and increase in size with increasing number, k, of iron ions within. Soluble iron corresponds to the smallest iron 'particle', i.e. one iron ion surrounded by water molecules ($k = 1$). We consider iron particles from $k = 1$ up to $k = 10^{12}$ iron ions (figure 1), with corresponding radii, r_k, ranging from 0.1 nm to approximately the size of a cell, 1 µm, covering the range of colloid and particulate iron sizes present in marine environments; in open ocean waters, radii range from less than 10 nm up to at least 500 nm [8,11,12,19]. For reasons of mathematical tractability, we assume a homogeneous distribution of iron particles, i.e. all particles have the same k. By varying k, we can then isolate the effect of particle size on iron uptake.

We want to highlight that this model implements several simplifications in order to single out the effect of diffusion limitation in the complex marine system. In reality, iron particles are generally polymorphous, containing iron as well as hydroxide or other groups. Over time, and depending on external conditions like pH, the particles can change in crystal structure and size [43,44], factors that also influence iron solubility [16]. Here, we assume that iron aggregates exclusively contain iron ions and only change when dissolved directly by cells or siderophores. We do not consider other dissolution processes, e.g. proton-promoted dissolution, that might be indirectly influenced when siderophores bind iron, e.g. by decreasing the solution saturation state [16]. We also do not consider the fact that the majority of dissolved iron is bound to ligands, some of which might be siderophores themselves [7]. While these factors are undoubtedly important for understanding the overall iron distribution in the ocean, they do not directly influence our investigation into the effects of diffusion limitation.

2.2. Low iron solubility strongly decreases the rate of direct iron uptake

To establish a baseline reference for the iron uptake rate, we first consider a single cell that relies on secretion-independent uptake by direct physical contact with iron particles, mediated, for example, by cell-attached siderophores or receptors (figure 1, top). The cell can only take up iron it encounters directly; in the absence of any 'active' motion, this can only be mediated by random diffusion. The uptake of iron can thus be described as a set of diffusing particles in three dimensions with the cell at the origin acting as an absorbing sphere (see Methods).

The likelihood of encounter between a cell and iron depends on the effective diffusion coefficient, which is the sum of the diffusion coefficient of the cell, D_B, and of the iron, D_k. The more iron ions are contained in a particle (larger k), the larger the diameter of the particle and the smaller the diffusion coefficient, $D_k \sim k^{-1/3}$. As a consequence, the likelihood of encounter with the cell is smaller for larger particles (see Methods). Since generally $D_k \gg D_B$, the encounter rate of a k-particle for a single non-secreting cell with radius R_B is approximately

$$\varphi_k \approx 4\pi\rho_k R_B D_k \sim k^{-2/3}, \tag{2.1}$$

where $\rho_k = \rho_0/k$ is the background concentration of iron particles and ρ_0 is the total background concentration of iron. Before a cell can take up iron from a particle it encounters, it first needs to release iron ions from the particle. The detailed kinetics that describe such a bacterial-mediated dissolution of

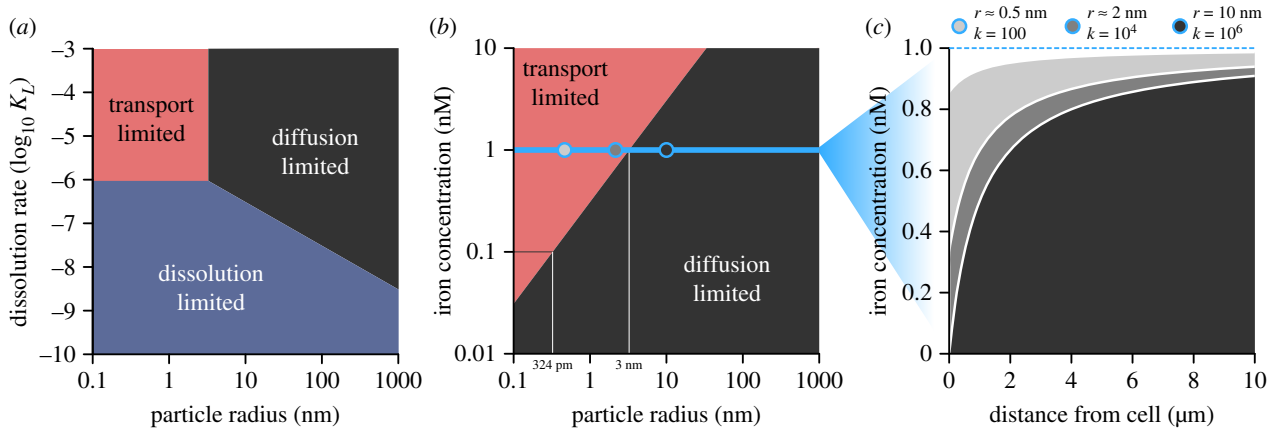

Figure 2. The level of iron aggregation, i.e. particle size, influences what process iron uptake is limited by. (*a*) When iron particles are large, the environment is generally diffusion limited, but transitions to dissolution limited as the dissolution rate decreases. As the particle sizes decrease, the environment becomes either transport limited for high dissolution rates or dissolution limited for low dissolution rates. Here, the background concentration of iron is $\rho_0 = 1$ nM. (*b*) The critical particle size for which the environment transitions from diffusion to transport limited (large κ_L) also depends on the background concentration of iron. As the size of iron sources increases at a given concentration, diffusion of iron slows down and eventually the iron at the cell surface is completely depleted. In this regime, all iron that arrives at the cell surface is immediately taken up, and the cell is limited by the amount of iron diffusing to the cell (diffusion limited, black area). The transition from transport-limited to diffusion-limited happens at increasing particle sizes as the background iron concentration increases (*ca* 324 pm for $\rho_0 = 0.1$ nM and 3 nm for $\rho_0 = 1$ nM). The blue line highlights the background concentration used for calculations leading to the data in (*c*) (0.1 nM). At this concentration, the threshold between the two types of limitation is at an aggregation level of $k = 33$. The radial iron concentrations at a background concentration of 1 nM (blue line) are shown for three particle sizes (blue circles) in (*c*). (*c*) The equilibrium iron concentrations as a function of the distance from the cell, with a background concentration of iron $\rho_0 = 1$ nM. For small particles (low *k*), in the transport-limited regime (red areas in (*a*,*b*)), the iron concentration at the cell surface decreases with increasing particle size, due to increasingly slow diffusion of iron, but iron is never completely depleted. In the diffusion-limited regime (black areas in (*a*,*b*)), iron is completely depleted at the cell surface, and thus the steady-state concentrations do not depend on the particle size anymore.

iron depends on the particular nature of the iron mineral (e.g. crystal structure) and the mechanism the bacteria employs to dissolve the mineral (surface ligands, reductases, etc.) [44,45]. Assuming cell-attached siderophores can bind to ions on the particle surface in a ligand exchange reaction and subsequently release iron ions from the crystal lattice at a rate κ_L, then the overall dissolution rate of a *k*-particle, ψ_k, will be proportional to the surface area of the particle, $S(k) \sim k^{2/3}$. The overall dissolution rate of the whole particle will then be $\psi_k \sim k^{-1/3}$, and based on geometric considerations can be approximated as (see Methods)

$$\psi_k \approx \frac{4}{3}\sigma\kappa_L k^{-1/3},$$

where κ_L is a pseudo-first-order rate constant and σ specifies the fraction of the surface area of the particle that a cell can sequester iron from. The balance between the encounter rate of new particles and their dissolution rate will determine whether cell-mediated dissolution can keep up with the influx of new iron.

We distinguish between three environmental regimes that limit the iron uptake of a cell under direct encounter (figure 2*a*) that are the result of one of the three key processes involved in iron uptake becoming the limiting process (figure 1): (1) in a *transport-limited* environment, the cell is producing enough soluble iron in the proximity of the cell, but the overall uptake is limited by the amount of iron that can be processed by the transporters at the cell surface; (2) in a *dissolution-limited* environment, the cell encounters iron particles more rapidly than it can dissolve them; (3) in a *diffusion-limited* environment, the cell has enough transporter and dissolution ability, but the encounter rate with new particles is too low. Iron aggregation influences both the concentration of iron at the cell surface, as well as the rate at which the particles are dissolved, as a function of $k^{1/3}$. Thus, depending on the dissolution rate, κ_L, the environment transitions from diffusion-limited when iron particles are large to either transport-limited (large κ_L) or dissolution-limited (small κ_L).

At iron concentrations that are realistic for open ocean waters, $\rho_0 = 0.1$–1 nM, diffusion limitation already occurs at particle sizes of $r \geq 0.3$ nm to 3 nm, depending on the background iron concentration (figure 2*b*). We determined the equilibrium distribution of iron particles by solving the spherically symmetric diffusion process (see Methods and [21]). The distribution of particles at steady state (figure 1*c*) for $\rho_0 = 1$ nM illustrates that in the transport-limited (or also dissolution-limited) regime, iron is never completely depleted at the cell surface, even though the iron concentration decreases towards the cell surface. By contrast, in a diffusion-limited regime, iron is completely depleted at the cell surface and only approaches background concentration levels at a distance of over four cell radii.

Under these conditions, the required time for a cell to encounter, dissolve, and take up sufficient iron to divide can reach up to days, for particles of size $r_k \approx 1$ nm, or months, for $r_k > 10$ nm. The time to division increases further with decreasing dissolution rate, κ_L (see Methods; electronic supplementary material, figure S1). The generation time of marine bacteria has been estimated to generally be on the time scale of days [46,47], which is much faster than predicted by our model for a cell only using direct uptake. This suggests that other mechanisms, such as for example siderophore secretion, are necessary to reach environmentally realistic growth rates.

The extremely long iron acquisition times are due to two difficulties that cells face under direct iron uptake. First, the rate at which cells encounter iron particles is low due to

the slow diffusion of the particles. Second, once cells encounter particles, larger particles are dissolved more slowly than smaller particles due to a lower surface-to-volume ratio (see Methods). Thus, although a cell will eventually 'gather' enough iron particles to reach a maximally possible uptake rate under the constraints set by the diffusion of the available iron, this maximum is only reached after extremely long time periods. For example, for particles of sizes around 5 nm, a cell starting from scratch would require over 4 years to reach the maximum uptake rate, although it would have already taken up enough iron to divide by around 6 months (see electronic supplementary material, figure S2). However, even if the cell were already taking up iron at its maximal rate—for example, by maintaining a reservoir of iron particles or by immediately dissolving the particles upon encounter ($\kappa_L \to \infty$)—it would still require around a month to take up enough iron to divide. Thus, a main consequence of low iron solubility is that cells can suffer from strong diffusion limitation, even at high iron concentrations. Cells might face similar problems in the uptake of nutrients from other larger substrates, such as particulate carbon sources.

Transport limitation can be alleviated at the cell membrane, for example through more efficient or more numerous transporters. Dissolution limitation due to low rates can in part be alleviated at the cell level by increasing the dissolution activity of membrane-bound ligands or reductases. But, both diffusion limitation and dissolution limitation due to limited processing space around the cell can only be overcome by processing iron away from the cell. Secreted molecules like siderophores can modify iron sources and alter their transport properties to both increase diffusion and accelerate uptake when encountered by a cell (figure 1, bottom). In the following, we will hence quantify the effect of siderophore secretion on overcoming diffusion limitation—by increasing the diffusion speed of iron—and dissolution limitation—by increasing the number of iron particles that can be processed in parallel.

2.3. Secreted siderophores can transiently increase the uptake rate of iron from large particles by accelerating diffusion

We next investigated whether siderophore secretion could alleviate diffusion and dissolution limitation. In addition to the diffusion of iron, we accounted for free (unbound) siderophores that are produced at the cell surface and diffuse away from the cell, as well as the reaction of free siderophores with iron resulting in siderophore–iron complexes outside the cell (figure 1). These complexes diffuse freely and can be taken up by the cell upon an encounter. We model these processes using a set of reaction–diffusion equations that describe the radial concentrations of iron particles, F, free siderophores, X, iron–siderophore complexes, Y, and particle surface ions bound by siderophores, E (see Methods). In order to investigate the direct effects of iron uptake mediated by secreted iron chelators, we excluded the possibility that cells take up free, unbound iron in these calculations.

Because siderophore–iron complexes are smaller than most iron particles, their diffusion coefficients are generally larger than those of the particles. This leads to accelerated diffusion that could potentially mitigate the limitation caused by the slow movement of large iron particles. Furthermore, the scavenging of iron from particles by siderophores is not limited to direct contact of the cell with the iron source. Thus, siderophores are able to solubilize iron from a larger number of iron sources simultaneously.

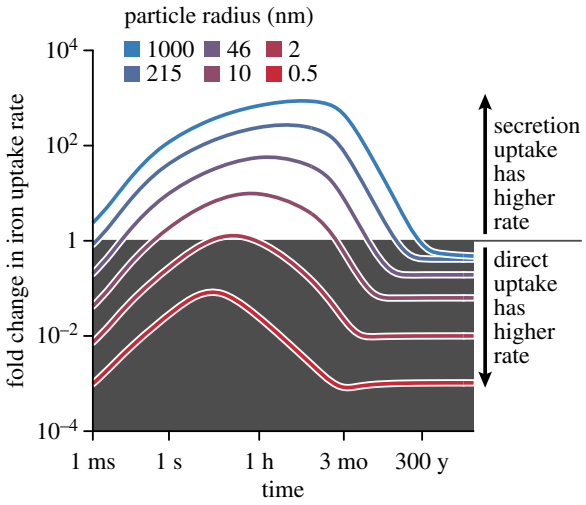

Figure 3. Siderophore secretion can strongly increase iron uptake over long time periods when iron is aggregated. The lines show the fold change in iron uptake rate for cells that secrete siderophores at a rate $P = 4.5 \times 10^{-2}$ amol h^{-1} compared to direct iron uptake. Iron particles are dissolved at a rate $\kappa = 10^6$ s^{-1}. Secretion uptake is initially slower than direct uptake until the concentration of adsorbed siderophores builds up. For large particles, secretion uptake surpasses direct uptake, reaching 100–1000 fold increases in the iron uptake rate. Eventually, secretion uptake decreases to comparable levels as direct uptake. However, the increase in uptake speed can last days or years, depending on the particle size.

The effects of secreting siderophores depend both on the size of the iron particle and whether the system is still in a transient phase or has already reached steady state. In the presence of large iron particles ($r_k > 10$ nm; the colloidal range) siderophore secretion indeed results in an uptake rate that quickly surpasses that of direct uptake for extended periods of time (figure 3). As the cell starts to produce siderophores, these quickly diffuse and bind to the surface of slowly moving particles at distances around the cell of up to a few centimetres (electronic supplementary material, figures S4 and S5). This leads to an initial increase in the iron uptake rate, within the first seconds under our conditions (figure 3). These adsorbed siderophores then contribute to the dissolution of all the iron particles in a relatively large volume around the cell. Siderophore–iron chelates are released from particles over time and a fraction of these quickly diffuse back to the cell. The long-term direct uptake rate eventually approaches and even slightly surpasses the secretion uptake rate, but this only happens over extremely long time periods (months to years), as a cell using direct uptake must first accumulate a reservoir of particles to degrade. The transient increase thus likely comprises many bacterial generations [46,47]. Overall, siderophore secretion increases the iron uptake rate compared to direct uptake, however, only during a—potentially very long—transient phase, and this transient increase in the uptake rate directly results in a large increase in the amount of iron acquired (electronic supplementary material, figure S3).

If iron is present in soluble form or as small particles ($r_k <$ 10 nm) the equilibrium uptake rate reached via siderophore secretion is mostly far below the direct uptake rate: releasing siderophores slows down iron acquisition. In this regime, the *fast diffusion limit*, the diffusion speed of iron is sufficiently

high that the background concentration of iron can be assumed constant (see Methods, equation (4.15)). Secretion slows down uptake because of two factors. First, siderophores must encounter iron and bind it, introducing an additional step prior to uptake. Second, the diffusion speed of siderophore–iron complexes is lower than that of free iron for $k < 1000$, thus reducing the flux of bound iron towards the cell. For very small iron particles (highly soluble iron), siderophore secretion results in slower acquisition than direct uptake. Therefore, for particle sizes greater than 0.3 nm but smaller than 10 nm (at an iron concentration of 0.1 nM and a dissolution rate of $\kappa_L = 10^6$), the cell is diffusion-limited, but secretion of siderophores is not effective at overcoming this limitation.

To access poorly soluble iron, cells could also—instead of secreting siderophores—increase their own diffusion coefficient by engaging in swimming motility. However, in such cases, it would be unlikely that a cell could dissolve more than one particle at a time. The rate at which a cell first encounters and subsequently dissolves single particles is a function of both the rate at which a non-motile cell encounters iron particles, ϕ_k, and the rate at which it dissolves the particle, ψ_k, leading to an overall rate $\phi_k\psi_k/(\psi_k + \phi_k)$. An increase in cell motility can potentially increase the encounter rate of new particles, ϕ_k, but because $\psi_k \ll \phi_k$, further increases in the encounter rate will only have marginal effects on the compounded iron uptake rate.

2.4. The effect of siderophore secretion depends on siderophore production rate and particle size

The increased iron uptake rate achieved by secretion in the presence of large iron particles, although only transient, can shorten the time necessary until a cell has acquired enough iron to initiate cell division significantly, from over a year for direct uptake to a few weeks with siderophore secretion (assuming an iron content of 10^6 Fe atoms $= 1.66$ amol per cell [36]; see also electronic supplementary material for a detailed discussion). In addition, we find that the siderophore production rate has a strong influence on the parameter range in which secretion-based uptake is superior to direct uptake, and that very high production rates are necessary to overcome diffusion limitation efficiently (electronic supplementary material, figure S6). The cost of producing such a high number of siderophores is difficult to estimate, since the negative effect of siderophore production on growth, due to resources spent on production instead of cell division, likely depends on environmental parameters such as the level of resource limitation [48]. However, to obtain an estimate of the magnitude and efficiency of siderophore production, we calculated how many siderophore molecules need to be produced in order to take up one iron ion (a similar approach to Völker & Wolf-Gladrow [21]). For a low siderophore secretion rate of 0.045 amol h^{-1} and a particle size of $r_k = 100$ nm, a secreter must release just under 28 000 siderophores to take up one iron ion, or a total of 47 femtomoles to divide. However, this seemingly high cost in terms of produced siderophores results in a significant reduction of the time necessary for acquiring enough iron to produce a daughter cell, from 354 days to 43 days at an iron concentration of $\rho_0 = 0.1$ nM. Faster uptake is achieved through higher siderophore secretion rates, though this also implies that more siderophores per iron are secreted: a secretion rate of 4.5 amol h^{-1} results in a division time of 26 days, requiring around 180 000 secreted siderophores per iron taken up at an iron concentration of $\rho_0 = 0.1$ nM and for $r_k = 100$ nm.

2.5. Synergistic siderophore production between two neighbouring cells can occur over a wide range of parameters

High siderophore production rates likely require a substantial investment of cellular resources. One way to reduce the production effort is cooperative production of siderophores in groups of cells. Siderophore–iron chelates that never return to one secreter cell might still benefit a different neighbouring cell. Furthermore, if cells can share their siderophores, each cell might have to produce fewer siderophore molecules overall. The outcome of such interactions is not easily predictable, though, since any increase in benefit from additional siderophores might be offset by having to share the incoming iron-bound chelates.

Siderophore production in a group of cells has been shown to increase the efficiency of accessing iron-bound siderophores thanks to an accumulation of siderophores in the neighbourhood of the cells [21]. However, these results did not consider the effect of large colloidal and particulate iron sources. In our model (for details, see Methods; electronic supplementary material, figure S7), we observe that—especially in the case of large iron sources—siderophore production affects and alters the environment in a large neighbourhood around the cell. Iron-bound siderophore chelates build up at distances of several hundred micrometres (see electronic supplementary material, figure S4), thus potentially allowing for cooperative interactions between cells located at significant distances. Our model indicates that both costs and benefits are influenced by the size of iron sources. First, achieving fast uptake from large iron aggregates requires a high siderophore-to-iron expenditure ratio, indicating that an important proportion of siderophores is lost to the producer cell even if no other cell is present. Thus, direct costs of sharing may be minimal if iron is present in large particles. Second, the benefits of sharing siderophore production with a producing neighbour cell are influenced by the beneficial returns of increasing siderophore production rate (electronic supplementary material, figure S6b).

We investigated a first stage of growth in a group of cells by considering the interactions between two cells. We measured the average number of siderophores produced by a secreter cell per iron taken up during the uptake time. The net effect of growing in proximity to another cell depends on how much a cell suffers from competition for iron-bound siderophores compared to how much it benefits from the siderophores produced by its neighbour. If sharing siderophores is synergistic, i.e. more efficient in a group, a cell has to produce fewer siderophores to take up one iron ion when a producing neighbour is present. We first quantified how much a siderophore-secreting cell is negatively influenced by the presence of a second cell by implementing this cell as an iron–siderophore chelate sink (comparable to cheater cells in [1]). We assume that the second cell does not produce siderophores, but still can take up iron bound to siderophores (but not free iron). We measure the negative effect (or cost) in terms of how many more siderophores the secreter cell needs to produce on average to take up one iron, relative to a situation

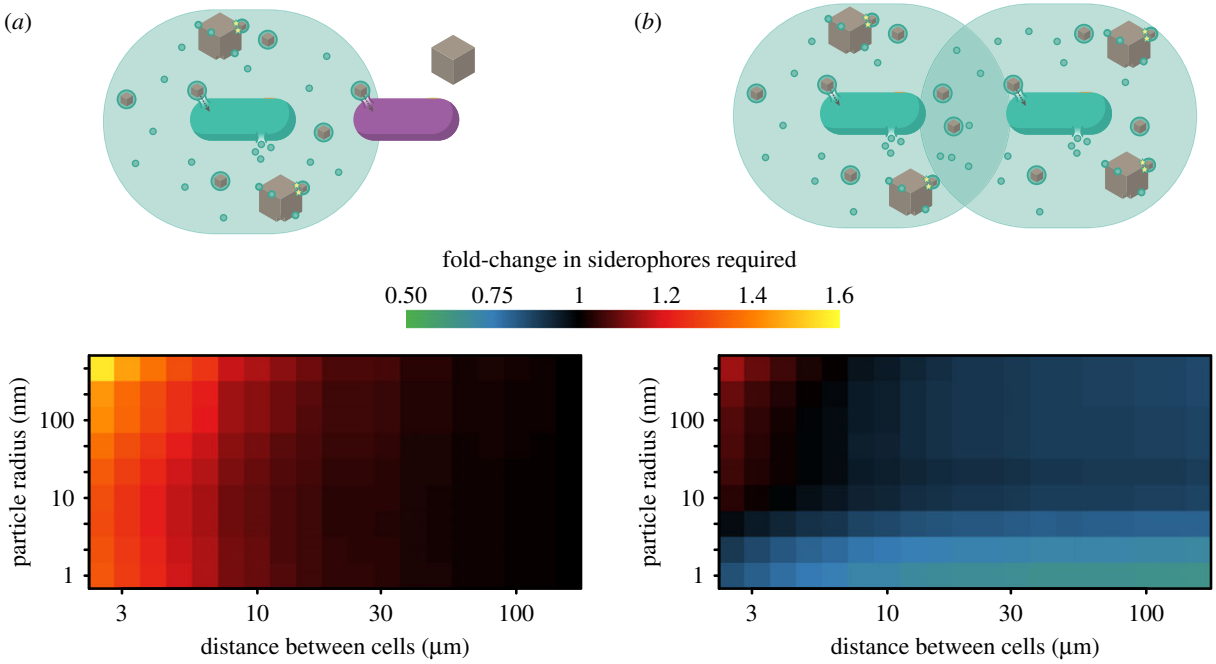

Figure 4. The length scale of competition for incoming iron–siderophore complexes is much shorter than the length scale of synergistic production of siderophores. (*a*) Only the secreter produces siderophores, the non-secreter consumes iron-bound siderophores, but does not contribute to production. The relative increase in the average number of siderophores that need to be produced to take up one iron, relative to if the secreter was alone, depends on the distance between the cells. When the two cells are close, the amount of siderophores required increases significantly (orange area). However, when cells are at distances of greater than 30 μm, the secreter does not need to produce additional siderophores (black area). The non-secreter generally acquires equal amounts of iron as the secreter. (*b*) Both cells produce siderophores. Secreters can increase the uptake rate of a neighbouring secreter at no or little additional cost, provided that the distance between cells is large enough. For small particles, the presence of an additional cell decreases the number of required siderophores by half, thereby alleviating the disadvantage of siderophore uptake for small particle sizes compared to direct uptake. The benefit is slightly reduced for larger aggregates, but remains synergistic and augments the benefit of secretion compared to direct uptake. Here, $\kappa_L = 10^{-6}$, $P = 0.045$ amol h^{-1}.

where no other cell were present. We find that, while the degree of iron aggregation does not strongly influence the interaction, the distance between the cells plays a key role (figure 4*a*). If the two cells were (hypothetically) at the exact same point in space, then all iron–siderophore chelates that arrive at the cells are shared evenly between the two, and the producing cell needs to produce many more siderophores, and increasingly so the larger the particles. As the distance between the two cells increases, the negative effect on the producer decreases (figure 4*a*). The loss of siderophores to the neighbouring cell at distances larger than 10 μm has a negligible effect on the producing cell (electronic supplementary material, figure S8). At the same time, at these distances, the non-producing cell is able to take up almost equivalent levels of iron as the secreting cell. Thus, siderophores can efficiently be taken up by the neighbouring cell at a very low cost to the producer, because the non-producer benefits from the siderophores that would likely be lost to the producer anyway.

Because the benefits of siderophore secretion can be shared with neighbouring cells at relatively short distances without additional costs to the producing cell, we next examined how joint secretion may be synergistically beneficial for cells. We measure benefit here as a reduction in the amount of siderophores secreted to achieve uptake of one iron ion. Values smaller than 1 mean that both cells benefit from the presence of another producer, because they efficiently share siderophores. As a result, each cell has to secrete fewer siderophores to take up the same amount of iron.

Highly soluble and insoluble iron sources enable synergistic interactions, whereas medium-sized aggregates do not. Over a large range of separation distances (greater than 10 μm for $P = 0.045$ amol h^{-1}), cells can share the benefits of secretion without an additional cost due to competition (blue-green areas in figure 4*b*), and cooperative effects are thus greater than competitive effects. The magnitude of the synergistic effect, however, depends on the marginal benefit of increased siderophore production rate (i.e. the slope in figure S6b in the electronic supplementary material). For production levels that only result in a small increase in iron uptake, the marginal benefit of an additional producer cell is small (black areas in figure 4*b*). The outcome of social interactions is therefore strongly influenced by the physical properties of iron, in particular the diffusion coefficient.

Overall, we find that at the majority of our conditions, siderophore secretion can lead to synergistic interactions between two neighbouring siderophore producing cells. This aids in making the secretion of siderophores a favourable strategy in a wide range of environments compared to direct uptake (figure 4*b*).

3. Discussion

The ubiquity of bacterial siderophore secretion despite the risk of siderophore loss and the evolutionary fragility it entails has stimulated a large body of research [1,49,50]. Here, we suggest that the release of siderophores is important for their function, potentially explaining why this uptake strategy is so widespread. We show that low iron solubility, present in many environments, can strongly slow down iron uptake if no siderophores are released, simply because the majority of iron sources occur in particles that diffuse slowly. Secreted

siderophores solubilize iron and generate small chelates with significantly increased diffusion speed. When we estimate the beneficial effect of siderophores in the marine environment, we find that siderophore release can significantly increase iron uptake speed on a time scale of months. While our model is a highly simplified version of marine iron chemistry, we think that it can contribute to our understanding of beneficial effects that require release of siderophores, namely for the role of overcoming diffusion limitation.

Recently published data suggest that amphiphilic siderophores constitute the majority of siderophores in the ocean [26], which might appear contradictory to the predictions of our model. Amphiphilic siderophores are often viewed as the result of an evolutionary adaptation to the dilute marine environment that minimize diffusive loss by remaining associated with the producing cell rather than being secreted [28,30]. In this case, the maximal number of siderophores that can be produced by a cell is limited by the cell surface area, unlike secreted hydrophilic siderophores, which would strongly reduce the functionality of siderophores with respect to diffusion limitation for iron uptake. We suggest several explanations to address the apparent mismatch between the measurements of amphiphilic siderophores in the ocean and our model. First, quantitative data on the relative concentrations of hydrophilic compared to amphiphilic siderophores are limited and understanding the broad distributions of marine siderophore pools still requires further investigation. Second, amphiphilic siderophores need not represent a 'non-secreter' iron uptake strategy as we model it here. Chemical structures of amphiphilic siderophores vary considerably and as a result these siderophores do not necessarily stay associated with the cell. Aquachelins and marinobactins A–E, for example, are isolated from the supernatant of laboratory cultures rather than the pellet [27], suggesting that they are secreted by the cells. Thus, at least some of the amphiphilic siderophores measured in the oceans are likely also secreted siderophores. Third, hydrophilic, i.e. unambiguously secreted, siderophores have frequently been isolated from marine environments [26,51,52]. In reality, bacteria will likely employ a combination of different secreted and non-secreted iron uptake strategies to maximize iron acquisition.

Siderophores are also believed to be important drivers of competitive interactions between unrelated genotypes. The chemical diversity of siderophores allows siderophore-bound iron to often be 'reserved' for the siderophore producer and is only poorly accessible to other genotypes [53]. The biological basis is that uptake of siderophore-bound iron requires a transporter specific to the structure of the siderophore. In our model, we only consider the case where the 'cheating' genotype is able to access siderophore-bound iron (figure 4), as has previously been observed for marine bacterial communities [54]. Nevertheless, access to iron can be restricted once it is chelated to a siderophore and thus impede growth of competitors [55]. Successful 'reservation' of environmental iron is not possible if siderophores stayed attached to the cell, thus further contributing to the benefits of secretion. These effects with respect to competition do not preclude the benefits with respect to diffusion that we describe here, suggesting that siderophore secretion might fulfil multiple roles.

Siderophore secretion is often cited as one of the central examples for diffusible public goods in the study of the evolution of cooperation [1,25,56,57]. Secreted molecules, such as siderophores, are at risk of being 'stolen' by a cheater genotype that avoids the cost of production, but reaps the benefits. The current consensus is that cooperation by means of secreted public goods is stabilized by spatially structured environments, as this increases the probability of interactions between identical genotypes, and consequently decreases the probability of interactions between producers and cheats [56–59]. Only few of these studies, however, have considered the process of diffusion of the public good to the full extent [57,60–63]. More importantly, game-theoretical studies mostly model the diffusive public good itself as a carrier of some benefit [57,63]. In our study, we consider a more realistic view of the mechanism of siderophore-based iron uptake. A secreted siderophore *per se* is useless to the cell, and any neighbouring cell, until it encounters and chelates iron.

In addition to findings on the importance of siderophores for mediating diffusion limitation, our model also reveals that abiotic properties of the substrate, in this case the diffusivity of iron, can play an important role in social interactions between cells, and need be taken into account when considering cooperative dynamics. The same also applies to other secreted metabolites that interact with large slow substrates, such as chitinases secreted to degrade chitin, or other extracellular degrading enzymes (cellulase, exoprotease).

We suggest that when analysing microbial competition and cooperation in these release-based uptake strategies, it is important to consider two different length scales: (1) the length of competition, i.e. the distance between neighbouring producers at which they compete for the shared resource, in this case the iron-bound siderophores; and (2) the length of synergism, i.e. the distance at which the neighbouring producers synergistically use the siderophores produced. Our model shows that typically the length scale of competition is much shorter than the length scale of synergism. This allows neighbouring producer cells to jointly increase the global siderophore production without paying additional costs due to competition. Thus, the benefits of siderophore secretion increase with the number of cells, while the costs per cell stay constant, if the cells are sufficiently spaced. This could set the basis for successful cooperative interactions in the secretion of many compounds.

Marine particles are a specific environment that might favour secretion-based iron uptake in the ocean. Cells can attach and grow in groups, establishing the infrastructure for synergistic interactions. In addition, growth on a particle containing organic matter might provide plentiful resources that can be channelled into production of siderophores. Copiotrophic microorganisms, especially, might experience conditions that are highly favourable for siderophore secretion. Indeed, an increased capacity for siderophore production has previously been linked to copiotrophs [32,64].

Release-based nutrient uptake, such as the secretion of siderophores or enzymes, has stimulated intense research in evolutionary and environmental microbiology, because of the seemingly fragile efficacy: releasing a metabolite entails a risk of loss and can be considered an immense task of 'environmental engineering' as resources outside of the cell are transformed on a large scale. Here, we have focused on the specific prominent example of the secretion of siderophores in the ocean and showed that secretion conveys an especially large benefit if the nutrient of interest—in this case, iron—is hard to reach. However, because the benefits of secretion lie in modulating the diffusive properties of the resource, rather than the specific chemical interaction, we expect our results to apply to any secreted foraging strategy where cells and resource are

physically separated. We suggest that the benefits of secretion in increasing the resource availability can outweigh these costs—especially in groups—and help us understand why bacteria frequently engage in release-based nutrient uptake.

4. Methods

4.1. Direct uptake

4.1.1. Encounter rate

If we assume a spherical cell with radius r_B, then the probability that a spherical iron particle starting at a distance r from the cell encounters the cell before time t is just the hitting probability of a random walk [65,66]

$$p_{\mathrm{col}}(r) = \frac{R}{r}\,\mathrm{erfc}\left(\frac{r-R}{\sqrt{4Dt}}\right), \tag{4.1}$$

with total radius $R = r_B + r_{\mathrm{Fe}}$ and effective diffusion coefficient $D = D_B + D_{\mathrm{Fe}}$. The diffusion coefficient is $D = k_B T/6\pi hr$, where $k_B \approx 1.38 \times 10^{-23}$ J K^{-1} is Boltzmann's constant, $T = 293$ K is ambient temperature, $h = 1.003$ mPa s is the viscosity of water at ambient temperature, and r is the radius of the spherical particle in metres. By summing the diffusion coefficients to an effective diffusion coefficient, we fix the reference frame of the iron particle to the bacterium and subsume the movement of the bacterium into the movement of the iron particle. As a simplification, we assume that the cell is stationary in space, and thus the effective diffusion coefficient is $D \approx D_{\mathrm{Fe}}$. Note that generally iron diffusion is faster than diffusion of the cell, $r_B \gg r_{\mathrm{Fe}}$, so that in most cases $D_B + D_{\mathrm{Fe}} \approx D_{\mathrm{Fe}}$ is an acceptable approximation.

The total number of particles that have collided with the bacterium by time t is

$$N(t) = \int_{r=R}^{\infty} p_{\mathrm{col}}(r)\,\mathrm{d}n(r),$$

where $\mathrm{d}n(r)$ is the number of particles at a distance r. If the concentration of iron is ρ and the iron particles are equally distributed in space, then $\mathrm{d}n(r) = \rho \cdot 4\pi r^2\,\mathrm{d}r$. Thus the total number of particles becomes

$$N(t) = 4\pi\rho R \int_{r=R}^{r} \mathrm{erfc}\left(\frac{r-R}{\sqrt{4Dt}}\right)\mathrm{d}r.$$

We assume that all iron particles contain k Fe atoms and that the total concentration of iron is $\rho_0 = k \cdot \rho_k$, where ρ_k is the concentration of particles of size k. The number of particles of size k that have collided with the bacterium at time t is

$$N_k(t) = \rho_k\ t \cdot 4\pi R_k D_k\left(1 + \frac{2R_k}{\sqrt{\pi D_k t}}\right),$$

with $R_k = (r_B + k^{1/3} r_{\mathrm{Fe}})$ and $D_k = k_B T/(6\pi h \cdot k^{1/3} r_{\mathrm{Fe}})$. The instantaneous encounter rate between a cell and iron particles is thus

$$\varphi_k(t) = \partial_t N(t) \approx 4\pi\rho_k R_k D_k. \tag{4.2}$$

At best, a bacterium can immediately take up a whole k-particle, such that maximum possible iron uptake is $\phi_k(t) = k\varphi_k(t)$, which for large t is $\phi_k \approx 4\pi\rho_0\ R_B\ D_k$.

4.1.2. Dissolution

Generally, a cell will not be able to absorb a complete k-particle, but will first need to dissociate iron ions from the aggregate. Kraemer [10] studied the ligand-controlled dissolution of iron minerals and derived that the overall dissolution rate is

$$R_L = \kappa_L[L],$$

where k_L is a pseudo-first-order rate constant and $[L]$ is the concentration absorbed ligands that are bound to surface ions. Thus, the dissolution rate of a whole particle depends on the exposed surface area and will change over time. We assume that the rate constant for cell-controlled dissolution of iron is similar in order of magnitude, $\kappa_L \approx 10^{-6}\ \mathrm{s}^{-1}$.

For perfectly packed spherical particles of size k, a rough approximation of the number of ions that are on the sphere surface can be found as the ratio of the total sphere surface divided by the cross section of a single ion:

$$n_S(k) = \frac{4\pi r_k^2}{\pi r_1^2} = 4k^{2/3}.$$

In reality, $n_S(k)$ will depend on precise shape or crystal structure of the iron mineral. The dissolution of iron particles by cells will likely be slower than free ligand-controlled dissolution because surface-bound ligands or reductases will only be able to react with a subset, σ, of the particle surface:

$$n_S^*(k) = \sigma n_S(k).$$

As the particle is continuously dissolved, the surface to volume ratio increases, affecting the dissolution rate [67]. The expected dissolution time of an idealized k-particle would be

$$T_k^{(\mathrm{diss})} = \int_{k'=1}^{k} \frac{1}{\kappa_L n_S(k')} = \frac{3}{4\sigma\kappa_L}(k^{1/3} - 1).$$

Thus, an upper bound for the rate at which a cell might dissolve an aggregate for $k \gg 1$ is thus

$$\psi_k = \frac{1}{T_k^{(\mathrm{diss})}} \approx \frac{4}{3}\sigma\kappa_L k^{-1/3}.$$

4.1.3. Uptake

We assume that a cell can maintain 'hold' of a reservoir of iron aggregates it encounters as it is dissolving them (figure 2). The amount of iron aggregates, $I_k(t)$, that are currently being processed by the cell then is determined by the number of aggregates that arrived due to diffusion, $\varphi_k(t)$, and the rate at which the aggregates are dissolved by the cell, $\psi_k(t)$:

$$\frac{\mathrm{d}I_k}{\mathrm{d}t} = \varphi_k(t) - \psi_k(t) I_k(t). \tag{4.3}$$

Assuming that the dissolved iron is fully sequestered by the cell, the total amount of iron that is taken up into the cell follows

$$\frac{\mathrm{d}A}{\mathrm{d}t} = k\psi_k I_k.$$

Using the approximation that φ_k is constant through time, $I_k(t)$ has a simple solution

$$I_k(t) = \frac{\varphi_k}{\psi_k}(1 - \mathrm{e}^{-\psi_k t}),$$

and, hence, the actual flux of iron into the cell is

$$\alpha_k = \frac{dA}{dt} = \phi_k(1 - \mathrm{e}^{-\psi_k t}). \tag{4.4}$$

The exponential term implies that the cell may eventually reach an iron uptake rate that is the same as the influx of new iron, but depending on the dissolution rate of aggregates, ψ_k, this maximum is only reached slowly.

Note that the maximal uptake flux given by equation (4.4) can only be achieved if the cell is able to concurrently process the required amount, $I_k(t)$, of iron particles, which requires physical attachment to the aggregate. Equation (4.3) implies that the maximum number of iron particles that are processed by the cell simultaneously is

$$I_k^{(\max)} = \frac{\varphi_k}{\psi_k} = 3\pi\frac{\rho_0}{k}\frac{R_k D_1}{\sigma\kappa_L}.$$

Owing to spacial constraints, the maximum number of aggregates that can surround a cell of radius R_B is roughly

$$n_B(k) = \frac{4\pi R_B^2}{\pi r_k^2} = 4\left(\frac{R_B}{r_1}\right)^2 k^{-2/3}.$$

Thus, under the assumption that cells can completely surround themselves with iron aggregates, the necessary background concentration of iron to saturate the cell's dissolution ability is

$$\rho_0^* = \frac{4R_B}{3\pi r_1^2 D_1}\sigma\kappa_L k^{1/3},$$

where the iron uptake rate under dissolution saturation is

$$\alpha_B = k\psi_k n_B(k) = \frac{16}{3}\left(\frac{R_B}{r_1}\right)^2 \sigma\kappa_L.$$

We say that the cell is iron-diffusion limited if the maximal flux is smaller than the maximally possible transport rate, i.e. $\lim_{t\to\infty}\alpha_k(t) = \phi_k < \alpha_T$ (figure 2*b*).

Finally, the total amount of iron that is actually taken up by the cell starting with $A(0) = 0$ is

$$A(t) = \phi_k\left(t + \frac{e^{-\psi_k t} - 1}{\psi_k}\right), \tag{4.5}$$

and the time, τ, required to take up a set amount of iron, A_0, is then the solution to $A(\tau) = A_0$.

4.1.4. Radial concentration

The concentration of iron aggregates, $F_k(r, t)$, can be equivalently represented as a spherically symmetrical diffusion process:

$$\frac{\partial F_k}{\partial t} + \frac{1}{r^2}\frac{\partial}{\partial r}\left(r^2 D_k \frac{\partial F_k}{\partial r}\right) = 0, \tag{4.6}$$

with an absorbing boundary at $r = R_k$, a reservoir at infinity, $\lim_{r\to\infty} F_k(r, t) = \rho_k = \rho_0/k$, and initial concentration $F_k(r, 0) = \rho_k$. The general equilibrium solution to equation (4.6) with $\partial_t F_k(r, t) = 0$ is $\tilde{F}_k(r) \equiv \lim_{t\to\infty} F_k(r, t) = \rho_k - c/r$. The constant c is found by the boundary condition at $r = R_k$. On the one hand we require $F_k(R_k, t) \geq 0$, and thus $c \leq R_k\rho_k$. On the other hand, the iron uptake is limited by the maximal transport or dissolution rate. For a fully absorbing boundary, the flux across the cell surface is

$$J_k = D_k(\partial_r\tilde{F}_k)|_{r=R_k} = \frac{D_k c}{R_k^2},$$

and thus the maximal flux for $c^{\max} = R_k\rho_k$ is $J_k^{\max} = D_k\rho_k/R_k = \varphi_k/(4\pi R_k^2)$, the same as the asymptotic limit of equation (4.2) divided by absorbing surface area. Under transport or dissolution limitation, $c_T = \alpha_T R_k^2/D_k$ and $c_B = \alpha_B R_k^2/D_k$, respectively.

4.2. Siderophore-mediated uptake

4.2.1. Reaction–diffusion equations

The iron uptake by a single secreting cell is modelled as a reaction–diffusion process for free iron, F, unbound siderophores, X, ligated surface ions, E, and bound siderophores, Y:

$$\frac{\partial F}{\partial t} = D_k\nabla^2 F - \kappa_X X(E_0 - E), \tag{4.7}$$

$$\frac{\partial X}{\partial t} = D_X\nabla^2 X - \kappa_X X(E_0 - E), \tag{4.8}$$

$$\frac{\partial E}{\partial t} = D_k\nabla^2 E + \kappa_X X(E_0 - E) - \kappa_L E \tag{4.9}$$

and

$$\frac{\partial Y}{\partial t} = D_X\nabla^2 Y + \kappa_L E. \tag{4.10}$$

Here, E_0 is total amount of ions at the surface of the iron aggregates, $E_0 = n_S(k)\cdot F/k = 4k^{-1/3}F$. When we only consider a single cell, the system is spherically symmetric, such that $\nabla^2 = r^{-2}\partial_r(r^2\partial_r)$ (see also [21]). When a free siderophore encounters an iron aggregate, it must first bind to an ion of iron at the aggregate surface,

$$\mathrm{Fe}^{\dagger} + \mathrm{X} \overset{a}{\rightleftharpoons} \mathrm{E} \overset{b}{\to} \mathrm{Y},$$

where $\mathrm{Fe}^{\dagger}$ refers to an unligated surface ion. Kraemer [10] describes this reaction as an adsorption reaction by ligand-exchange that proceeds forward with a pseudo second-order rate constant, κ_X. For high-affinity siderophores, κ_X is generally much higher than the reverse reaction rate, such that we ignore the reverse reaction, and use $\kappa_X = 10^6\,\mathrm{M}^{-1}\mathrm{s}^{-1}$. The pseudo-first-order rate constant, κ_L, describes the dissolution of the siderophore–iron complex from the crystal lattice, and is of the order of $\kappa_L \sim 10^{-2}\,\mathrm{h}^{-1} \sim 10^{-6}\,\mathrm{s}^{-1}$. Initially, iron is equally distributed in space at a concentration of $F(r, 0) = \rho_0$ and there are no siderophores present, $X(r, 0) = 0$. We assume that the concentration of free and bound siderophores tends to zero far away from the cell, $\lim_{r\to\infty} X(r, t) = Y(r, t) = 0$, and the concentration of iron is constant far away from the cell, $\lim_{r\to\infty} F(r, t) = \rho_0$. The uptake rate of iron–siderophore complexes by the cell is then just equal to the flux of Y at $r = R_B$:

$$J = D_X(\partial_r Y(r, t))|_{r=R_B},$$

with a maximal transport-limited rate of α_T as in the direct uptake case.

The system of reaction–diffusion equations cannot be solved analytically, but can be integrated numerically. To gain some analytical understanding of the equilibrium distributions, we consider some limiting cases of the reaction–diffusion system.

4.2.2. No reaction

In the absence of any reaction of siderophores with iron, $\kappa_X = 0$. In this case, the equilibrium solution for the distribution of free siderophores is

$$X^*(r) = \frac{PR_B^2}{D_X}\left(\frac{1}{r} - \frac{1}{R_\infty}\right),$$

where P is the excretion rate of siderophores from the cell. Here, R_∞ is the upper bound of the considered volume. For an open system, $R_\infty \to \infty$,

$$X^*(r) = \frac{PR_B^2}{D_X r}. \tag{4.11}$$

4.2.3. Large aggregation, slow dissolution

When the level of aggregation is large, then the diffusion of free iron is much slower than the diffusion of free siderophores. Furthermore, the dissolution of the ligated surface ions is generally slow, such that the distribution of free siderophores, $X(r)$, equilibrates with the bound surface iron, E. Assuming that the iron aggregates are stationary ($D_k = 0$), we can calculate the radial distribution of bound surface irons as the solution to

$$\frac{\mathrm{d}E(r)}{\mathrm{d}t} = \kappa_X X^*(r)(E_0 - E(r)) - \kappa_L E(r),$$

such that

$$E^*(r) = \frac{\kappa_X X^*(r)}{\kappa_X X^*(r) + \kappa_L}E_0. \tag{4.12}$$

From this we can derive a characteristic radius below which $E(r) \approx E_0$ when there is sufficient iron and above which $E(r)$

declines towards zero. Solving $E^*(R^*) = E_0/2$,

$$R^* = \frac{PR_B^2}{D_x}\frac{\kappa_X}{\kappa_L}.$$

4.2.4. Large aggregation, immediate dissolution

When the level of aggregation is large, then the diffusion of free iron is much slower than the diffusion of free siderophores. But since the concentration of siderophores decreases with distance from the cell as a consequence of the spherical dilution, there exists a boundary at $r = R^*$, where the influx of free siderophores completely reacts with the influx of free iron.

Let $\Delta X = \phi_X \Delta t$ and $\Delta F = \phi_F \Delta t$ be the amount of X and F that enters a finite small volume during time Δt. Then the amount that reacts will be $\Delta Y = \kappa \Delta F \Delta X$. We are interested in the case where all iron ΔF reacts with all siderophores ΔX, $k\Delta X \Delta F = \Delta F$ and $k\Delta X \Delta F = \Delta X$, and hence, $\Delta F = \Delta X$, or, $|\phi_X(R^*)| = |\phi_F(R^*)|$.

Iron diffuses to $r = R^*$ from above, and siderophores diffuse to $r = R^*$ from below. Thus for $r < R^*$, the distribution of free siderophores follows equation (4.11) with $R_\infty = R^*$. Equivalently, the distribution of iron for $r > R^*$ follows that of freely diffusing iron, $F(r) = \rho_0(1 - R^*/r)$. The fluxes are then

$$\phi_X(r) = \frac{PR_B^2}{r^2}$$

and

$$\phi_F(r) = -\frac{D_F \rho_0 R}{r^2}.$$

These are equal at

$$R^* = \frac{PR_B^2}{D_F \rho_0}. \tag{4.13}$$

This defines a boundary at a distance $r = R^*$ from the cell. Below this radius, there are enough siderophores to bind all free iron and thus there is no free iron. Above this radius, all the siderophores have been bound. Hence at equilibrium, siderophore–iron complexes are only produced at this radius.

The distribution of siderophore–iron complexes above $r = R^*$ then is

$$Y^+(r) = \frac{PR_B^2}{D_X r}.$$

Below $r = R^*$, $Y^-(r) = Y^*((1 - R_B/r)/(1 - R_B/R^*))$, where $Y^* = Y^+(R_*) = \rho_0 D_F/D_X$,

$$Y^-(r) = \rho_0 \frac{D_F}{D_X}\frac{PR_B}{PR_B - D_F\rho_0}(1 - R_B/r).$$

Finally, this results in a flux at the cell of

$$J_Y = \frac{\rho_0 D_F}{R_B - D_F \rho_0/P}. \tag{4.14}$$

This converges to the maximal direct uptake flux, $J = \rho_0\, D_F/R_B$, for secretion rates $P \gg D_F\rho_0$.

4.2.5. Fast diffusion, immediate dissolution

If the diffusion speed of free iron is fast compared to the reaction speed of siderophores, then the background concentration of free iron can be assumed constant. The reaction–diffusion equations then become

$$\frac{\partial X}{\partial t} = \frac{1}{r^2}\frac{\partial}{\partial r}\left(r^2 D_X \frac{\partial X}{\partial r}\right) - \kappa_0 X$$

and

$$\frac{\partial Y}{\partial t} = \frac{1}{r^2}\frac{\partial}{\partial r}\left(r^2 D_X \frac{\partial Y}{\partial r}\right) + \kappa_0 X,$$

with $\kappa_0 = \kappa\rho_0$. The equilibrium solutions to these equations for boundary conditions $\lim_{r\to\infty} X(r) = \lim_{r\to\infty} = 0$, $\phi_X(R_B) = -D_X \partial_r X(r = R_B) = P$ and $Y(R_B) = 0$ are (see [21])

$$X(r) = \frac{PR_B^2}{D_X r}\frac{e^{-(r-R_B)/L}}{1 + R_B/L} = X^*(r)\frac{e^{-(r-R_B)/L}}{1 + R_B/L}$$

and

$$Y(r) = \frac{PR_B^2}{D_X r}\frac{1 - e^{-(r-R_B)/L}}{1 + R_B/L} = X^*(r)\frac{1 - e^{-(r-R_B)/L}}{1 + R_B/L}.$$

Here, $L = \sqrt{D_X/\kappa_0}$ is the characteristic diffusion–reaction length of siderophores with the background iron. The derivative of Y is

$$\frac{\partial Y}{\partial r} = \frac{PR_B^2}{D_X(1 + R_B/L)r}\left(-\frac{1}{r}(1 - e^{-(r-R_B)/L}) + \frac{e^{-(r-R_B)/L}}{L}\right).$$

Hence, as derived in [21], the maximum iron uptake rate is

$$\phi_Y(R_B) = \frac{PR_B}{L + R_B}, \tag{4.15}$$

and the peak in the distribution is at a distance r, where

$$ye^{R_B/L - y} = 1, \quad y = r/L + 1. \tag{4.16}$$

4.3. Numerical integration of the partial differential equations

With exception of the single cell direct uptake case, no analytical solutions to the reaction–diffusion equations are available. We therefore numerically integrated the equations using a finite-elements approach implemented in the FEniCS project v. 2018.1.0.6 [68]. The FEniCS software suite uses the variational formulation of the PDEs on meshes.

4.3.1. Single cell

For the single cell case, we exploited the spherical symmetry and used a linear expanding mesh between $R_B = 1$ µm and $R_\infty = 10$ m, and $m = 400$ mesh intervals:

$$r_i = R_B + (R_\infty - R_B)\left(\frac{i\Delta r - R_B}{R_\infty - R_B}\right)^4, \quad i \in [0, m],$$

where $\Delta r = (R_\infty - R_B)/m$. We solved the PDEs over discrete increasing time steps, with $\Delta t_0 = 10^{-4}$ s and $\Delta t_{j+1} = 1.2\Delta t_j$, with a maximum time step of 1000 s (see also electronic supplementary material).

4.3.2. Two cells

In the two cell case, the system only has cylindrical symmetry along the axis that connects the two cells:

$$\frac{\partial F}{\partial t} = \frac{1}{r}\frac{\partial}{\partial r}\left(rD_F\frac{\partial F}{\partial r}\right) + D_F\frac{\partial^2 F}{\partial z^2} - \kappa FX,$$

$$\frac{\partial X}{\partial t} = \frac{1}{r}\frac{\partial}{\partial r}\left(rD_X\frac{\partial X}{\partial r}\right) + D_X\frac{\partial^2 X}{\partial z^2} - \kappa FX$$

and

$$\frac{\partial Y}{\partial t} = \frac{1}{r}\frac{\partial}{\partial r}\left(rD_X\frac{\partial Y}{\partial r}\right) + D_X\frac{\partial^2 Y}{\partial z^2} + \kappa FX.$$

We generated two-dimensional (z, r)-meshes using the following procedure: we first created a circular domain of radius $\rho_1 =$ 100 µm. We then removed two circular 'cells', with radius R_B and varying distance d from each other, from the domain. The domain was then converted to a mesh using FEniCS with a mesh size of 10, and subsequently refining all mesh elements within the circle $\rho = \rho_1/2$. The mesh was finally expanded to a full radius of $\rho_\infty = 0.1$ m, by adding concentric circles of $m_2 =$ 24 mesh points at increasing radii $\rho_{j+1} = \rho_j(1 + 2\pi/m_2)$. Finally, we integrated the two-dimensional reaction–diffusion equations

using an increasing time step, $\Delta t_0 = 10^{-2}$ s and $\Delta t_{j+1} = 1.2\Delta t_j$, with a maximum time step of 1000 s.

Data accessibility. All simulation code is available at https://bitbucket.org/gaberoo/IronDolfin.

Authors' contributions. All authors conceived the model, interpreted the results and wrote the paper. K.T.S. formulated the initial question and context. G.E.L. performed the simulations and mathematical calculations.

Competing interests. We declare we have no competing interests.

Funding. G.E.L. was supported by the Swiss National Science Foundation (162251) and the Human Frontier Science Program (LT000643/2016-L). K.T.S. and M.A. were supported by Eawag and ETH Zurich. K.T.S. was further supported by the Swiss National Science Foundation (grant no. PP2EZP3-162260).

Acknowledgements. We thank Thierry Sollberger for help with designing figures 1 and 4. We also thank Roman Stocker, Laura Sigg, Stephan Kraemer and Mak Saito for helpful discussions.

References

1. Griffin AS, West SA, Buckling A. 2004 Cooperation and competition in pathogenic bacteria. *Nature* **430**, 1024–1027. (doi:10.1038/nature02744)
2. Drescher K, Nadell CD, Stone HA, Wingreen NS, Bassler BL. 2014 Solutions to the public goods dilemma in bacterial biofilms. *Curr. Biol.* **24**, 50–55. (doi:10.1016/j.cub.2013.10.030)
3. Pakulski JD, Coffin RB, Kelley CA, Holder SL, Downer R, Aas P, Lyons MM, Jeffrey WH. 1996 Iron stimulation of Antarctic bacteria. *Nature* **383**, 133–134. (doi:10.1038/383133b0)
4. Hutchins DA, DiTullio GR, Zhang Y, Bruland KW. 1998 An iron limitation mosaic in the California upwelling regime. *Limnol. Oceanogr.* **43**, 1037–1054. (doi:10.4319/lo.1998.43.6.1037)
5. Cochlan WP. 2001 The heterotrophic bacterial response during a mesoscale iron enrichment experiment (IronEx II) in the eastern equatorial Pacific Ocean. *Limnol. Oceanogr.* **46**, 428–435. (doi:10.4319/lo.2001.46.2.0428)
6. Paradkar PN, De Domenico I, Durchfort N, Zohn I, Kaplan J, Ward DM. 2008 Iron depletion limits intracellular bacterial growth in macrophages. *Blood* **112**, 866–874. (doi:10.1182/blood-2007-12-126854)
7. Boyd PW, Ellwood MJ. 2010 The biogeochemical cycle of iron in the ocean. *Nat. Geosci.* **3**, 675–682. (doi:10.1038/ngeo964)
8. Tagliabue A, Bowie AR, Boyd PW, Buck KN, Johnson KS, Saito MA. 2017 The integral role of iron in ocean biogeochemistry. *Nature* **543**, 51–59. (doi:10.1038/nature21058)
9. Braun V, Killmann H. 1999 Bacterial solutions to the iron-supply problem. *Trends Biochem. Sci.* **24**, 104–109. (doi:10.1016/S0968-0004(99)01359-6)
10. Kraemer S. 2004 Iron oxide dissolution and solubility in the presence of siderophores. *Aquat. Sci.* **66**, 3–18. (doi:10.1007/s00027-003-0690-5)
11. Wu J, Boyle E, Sunda W, Wen LS. 2001 Soluble and colloidal iron in the oligotrophic North Atlantic and North Pacific. *Science* **293**, 847–849. (doi:10.1126/science.1059251)
12. Fitzsimmons JN, Boyle EA. 2014 Both soluble and colloidal iron phases control dissolved iron variability in the tropical North Atlantic Ocean. *Geochim. Cosmochim. Acta* **125**, 539–550. (doi:10.1016/j.gca.2013.10.032)
13. Johnson KS, Gordon RM, Coale KH. 1997 What controls dissolved iron concentrations in the world ocean? *Mar. Chem.* **57**, 137–161. (doi:10.1016/S0304-4203(97)00043-1)
14. Hassler CS, Schoemann V, Nichols CM, Butler ECV, Boyd PW. 2011 Saccharides enhance iron bioavailability to Southern Ocean phytoplankton. *Proc. Natl Acad. Sci. USA* **108**, 1076–1081. (doi:10.1073/pnas.1010963108)
15. Salmon TP, Rose AL, Neilan BA, Waite TD. 2006 The FeL model of iron acquisition: nondissociative reduction of ferric complexes in the marine environment. *Limnol. Oceanogr.* **51**, 1744–1754. (doi:10.4319/lo.2006.51.4.1744)
16. Kraemer SM. 2005 Siderophores and the dissolution of iron-bearing minerals in marine systems. *Rev. Mineral. Geochem.* **59**, 53–84. (doi:10.2138/rmg.2005.59.4)
17. Bergquist BA, Wu J, Boyle EA. 2007 Variability in oceanic dissolved iron is dominated by the colloidal fraction. *Geochim. Cosmochim. Acta* **71**, 2960–2974. (doi:10.1016/j.gca.2007.03.013)
18. Fitzsimmons JN, Carrasco GG, Wu J, Roshan S, Hatta M, Measures CI, Conway TM, John SG, Boyle EA. 2015 Partitioning of dissolved iron and iron isotopes into soluble and colloidal phases along the GA03 GEOTRACES North Atlantic Transect. *Deep Sea Res. Part 2 Top. Stud. Oceanogr.* **116**, 130–151. (doi:10.1016/j.dsr2.2014.11.014)
19. von der Heyden BP, Roychoudhury AN, Mtshali TN, Tyliszczak T, Myneni SCB. 2012 Chemically and geographically distinct solid-phase iron pools in the Southern Ocean. *Science* **338**, 1199–1201. (doi:10.1126/science.1227504)
20. Hider RC, Kong X. 2010 Chemistry and biology of siderophores. *Nat. Prod. Rep.* **27**, 637–657. (doi:10.1039/b906679a)
21. Völker C, Wolf-Gladrow DA. 1999 Physical limits on iron uptake mediated by siderophores or surface reductases. *Mar. Chem.* **65**, 227–244. (doi:10.1016/S0304-4203(99)00004-3)
22. Hutchins DA, Rueter JG, Fish W. 1991 Siderophore production and nitrogen fixation are mutually exclusive strategies in Anabaena 712. *Limnol. Oceanogr.* **36**, 1–12. (doi:10.4319/lo.1991.36.1.0001)
23. De Vos D, De Chial M, Cochez C, Jansen S, Tümmler B, Meyer JM, Cornelis P. 2001 Study of pyoverdine type and production by *Pseudomonas aeruginosa* isolated from cystic fibrosis patients: prevalence of type II pyoverdine isolates and accumulation of pyoverdine-negative mutations. *Arch. Microbiol.* **175**, 384–388. (doi:10.1007/s002030100278)
24. West SA, Buckling A. 2003 Cooperation, virulence and siderophore production in bacterial parasites. *Proc. R. Soc. Lond. B* **270**, 37–44. (doi:10.1098/rspb.2002.2209)
25. Velicer GJ. 2003 Social strife in the microbial world. *Trends Microbiol.* **11**, 330–337. (doi:10.1016/S0966-842X(03)00152-5)
26. Boiteau RM, Mende DR, Hawco NJ, McIlvin MR, Fitzsimmons JN, Saito MA, Sedwick PN, DeLong EF, Repeta DJ. 2016 Siderophore-based microbial adaptations to iron scarcity across the eastern Pacific Ocean. *Proc. Natl Acad. Sci. USA* **113**, 14 237–14 242. (doi:10.1073/pnas.1608594113)
27. Martinez JS, Zhang GP, Holt PD, Jung HT, Carrano CJ, Haygood MG, Butler A. 2000 Self-assembling amphiphilic siderophores from marine bacteria. *Science* **287**, 1245–1247. (doi:10.1126/science.287.5456.1245)
28. Martinez JS, Carter-Franklin JN, Mann EL, Martin JD, Haygood MG, Butler A. 2003 Structure and membrane affinity of a suite of amphiphilic siderophores produced by a marine bacterium. *Proc. Natl Acad. Sci. USA* **100**, 3754–3759. (doi:10.1073/pnas.0637444100)
29. Xu G, Martinez JS, Groves JT, Butler A. 2002 Membrane affinity of the amphiphilic marinobactin siderophores. *J. Am. Chem. Soc.* **124**, 13 408–13 415. (doi:10.1021/ja026768w)
30. Kümmerli R, Schiessl KT, Waldvogel T, McNeill K, Ackermann M. 2014 Habitat structure and the evolution of diffusible siderophores in bacteria. *Ecol. Lett.* **17**, 1536–1544. (doi:10.1111/ele.2014.17.issue-12)
31. Hopkinson BM, Barbeau KA. 2012 Iron transporters in marine prokaryotic genomes and metagenomes. *Environ. Microbiol.* **14**, 114–128. (doi:10.1111/j.1462-2920.2011.02539.x)
32. Hogle SL, Thrash JC, Dupont CL, Barbeau KA. 2016 Trace metal acquisition by marine heterotrophic bacterioplankton with contrasting trophic strategies. *Appl. Environ. Microbiol.* **82**, 1613–1624. (doi:10.1128/AEM.03128-15)
33. Shaked Y, Lis H. 2012 Disassembling iron availability to phytoplankton. *Front. Microbiol.* **3**, 123. (doi:10.3389/fmicb.2012.00123)
34. Kuhn KM, DuBois JL, Maurice PA. 2013 Strategies of aerobic microbial Fe acquisition from Fe-bearing montmorillonite clay. *Geochim. Cosmochim. Acta* **117**, 191–202. (doi:10.1016/j.gca.2013.04.028)
35. Kranzler C, Kessler N, Keren N, Shaked Y. 2016 Enhanced ferrihydrite dissolution by a unicellular, planktonic cyanobacterium: a biological contribution

to particulate iron bioavailability. *Environ. Microbiol.* **18**, 5101–5111. (doi:10.1111/1462-2920.13496)

36. Andrews SC, Robinson AK, Rodriguez-Quiñones F. 2003 Bacterial iron homeostasis. *FEMS Microbiol. Rev.* **27**, 215–237. (doi:10.1016/S0168-6445(03)00055-X)
37. Marshall B, Stintzi A, Gilmour C, Meyer JM, Poole K. 2009 Citrate-mediated iron uptake in *Pseudomonas aeruginosa*: involvement of the citrate-inducible FecA receptor and the FeoB ferrous iron transporter. *Microbiology* **155**, 305–315. (doi:10.1099/mic.0.023531-0)
38. Sandy M, Butler A. 2009 Microbial iron acquisition: marine and terrestrial siderophores. *Chem. Rev.* **109**, 4580–4595. (doi:10.1021/cr9002787)
39. Miethke M, Marahiel MA. 2007 Siderophore-based iron acquisition and pathogen control. *Microbiol. Mol. Biol. Rev.* **71**, 413–451. (doi:10.1128/MMBR.00012-07)
40. Zhao CM, Campbell PG, Wilkinson KJ. 2016 When are metal complexes bioavailable? *Environ. Chem.* **13**, 425–433. (doi:10.1071/EN15205)
41. Worms I, Simon DF, Hassler CS, Wilkinson KJ. 2006 Bioavailability of trace metals to aquatic microorganisms: importance of chemical, biological and physical processes on biouptake. *Biochimie* **88**, 1721–1731. (doi:10.1016/j.biochi.2006.09.008)
42. Buffle J, Wilkinson KJ, Van Leeuwen HP. 2009 Chemodynamics and bioavailability in natural waters. *Environ. Sci. Technol.* **43**, 7170–7174. (doi:10.1021/es9013695)
43. Cornell RM, Giovanoli R, Schneider W. 1989 Review of the hydrolysis of iron(III) and the crystallization of amorphous iron(III) hydroxide hydrate. *J. Chem. Technol. Biotechnol.* **46**, 115–134. (doi:10.1002/jctb.280460204)
44. Schwertmann U, Friedl J, Stanjek H. 1999 From Fe(III) ions to ferrihydrite and then to hematite. *J. Colloid Interface Sci.* **209**, 215–223. (doi:10.1006/jcis.1998.5899)
45. Melton ED, Swanner ED, Behrens S, Schmidt C, Kappler A. 2014 The interplay of microbially mediated and abiotic reactions in the biogeochemical Fe cycle. *Nat. Rev. Microbiol.* **12**, 797–808. (doi:10.1038/nrmicro3347)
46. Jannasch HW. 1969 Estimations of bacterial growth rates in natural waters. *J. Bacteriol.* **99**, 156–160.
47. Kirchman DL. 2016 Growth rates of microbes in the oceans. *Ann. Rev. Mar. Sci.* **8**, 285–309. (doi:10.1146/annurev-marine-122414-033938)
48. Brockhurst MA, Buckling A, Racey D, Gardner A. 2008 Resource supply and the evolution of public-goods cooperation in bacteria. *BMC Biol.* **6**, 20. (doi:10.1186/1741-7007-6-20)
49. Kümmerli R, Brown SP. 2010 Molecular and regulatory properties of a public good shape the evolution of cooperation. *Proc. Natl Acad. Sci. USA* **107**, 18 921–18 926. (doi:10.1073/pnas.1011154107)
50. Dumas Z, Kümmerli R. 2012 Cost of cooperation rules selection for cheats in bacterial metapopulations. *J. Evol. Biol.* **25**, 473–484. (doi:10.1111/jeb.2012.25.issue-3)
51. Granger J, Price NM. 1999 The importance of siderophores in iron nutrition of heterotrophic marine bacteria. *Limnol. Oceanogr.* **44**, 541–555. (doi:10.4319/lo.1999.44.3.0541)
52. Vraspir JM, Butler A. 2009 Chemistry of marine ligands and siderophores. *Ann. Rev. Mar. Sci.* **1**, 43–63. (doi:10.1146/annurev.marine.010908.163712)
53. Kloepper JW, Leong J, Teintze M, Schroth MN. 1980 Enhanced plant growth by siderophores produced by plant growth-promoting rhizobacteria. *Nature* **286**, 885–886. (doi:10.1038/286885a0)
54. Cordero OX, Ventouras LA, DeLong EF, Polz MF. 2012 Public good dynamics drive evolution of iron acquisition strategies in natural bacterioplankton populations. *Proc. Natl Acad. Sci. USA* **109**, 20 059–20 064. (doi:10.1073/pnas.1213344109)
55. Schiessl KT, Janssen EML, Kraemer SM, McNeill K, Ackermann M. 2017 Magnitude and mechanism of siderophore-mediated competition at low iron solubility in the *Pseudomonas aeruginosa* pyochelin system. *Front. Microbiol.* **8**, 1964. (doi:10.3389/fmicb.2017.01964)
56. Kümmerli R, Griffin AS, West SA, Buckling A, Harrison F. 2009 Viscous medium promotes cooperation in the pathogenic bacterium *Pseudomonas aeruginosa*. *Proc. R. Soc. B.* **276**, 3531–3538. (doi:10.1098/rspb.2009.0861)
57. Allen B, Gore J, Nowak MA. 2013 Spatial dilemmas of diffusible public goods. *Elife* **2**, e01169. (doi:10.7554/eLife.01169)
58. Nadell CD, Foster KR, Xavier JB. 2010 Emergence of spatial structure in cell groups and the evolution of cooperation. *PLoS Comput. Biol.* **6**, e1000716. (doi:10.1371/journal.pcbi.1000716)
59. Julou T, Mora T, Guillon L, Croquette V, Schalk IJ, Bensimon D, Desprat N. 2013 Cell-cell contacts confine public goods diffusion inside *Pseudomonas aeruginosa* clonal microcolonies. *Proc. Natl Acad. Sci. USA* **110**, 12 577–12 582. (doi:10.1073/pnas.1301428110)
60. Vetter Y, Deming J, Jumars P, Krieger-Brockett B. 1998 A predictive model of bacterial foraging by means of freely released extracellular enzymes. *Microb. Ecol.* **36**, 75–92. (doi:10.1007/s002489900095)
61. Allison SD. 2005 Cheaters, diffusion and nutrients constrain decomposition by microbial enzymes in spatially structured environments. *Ecol. Lett.* **8**, 626–635. (doi:10.1111/ele.2008.8.issue-6)
62. Folse III HJ, Allison SD. 2012 Cooperation, competition, and coalitions in enzyme-producing microbes: social evolution and nutrient depolymerization rates. *Front. Microbiol.* **3**, 338. (doi:10.3389/fmicb.2012.00338)
63. Dobay A, Bagheri HC, Messina A, Kümmerli R, Rankin DJ. 2014 Interaction effects of cell diffusion, cell density and public goods properties on the evolution of cooperation in digital microbes. *J. Evol. Biol.* **27**, 1869–1877. (doi:10.1111/jeb.2014.27.issue-9)
64. Bundy RM, Boiteau RM, McLean C, Turk-Kubo KA, McIlvin MR, Saito MA, Van Mooy BAS, Repeta DJ. 2018 Distinct siderophores contribute to iron cycling in the mesopelagic at station ALOHA. *Front. Mar. Sci.* **5**, 61. (doi:10.3389/fmars.2018.00061)
65. Crank J. 1975 *The mathematics of diffusion*, 2nd edn. Oxford, UK: Clarendon Press.
66. Frazier Z, Alber F. 2012 A computational approach to increase time scales in Brownian dynamics-based reaction-diffusion modeling. *J. Comput. Biol.* **19**, 606–618. (doi:10.1089/cmb.2012.0027)
67. Schwertmann U. 1991 Solubility and dissolution of iron oxides. *Plant Soil* **130**, 1–25. (doi:10.1007/BF00011851)
68. Logg A, Mardal KA, Wells GN. 2012 *Automated solution of differential equations by the finite element method*. Berlin, Germany: Springer.
69. Alnæs M *et al.* 2015 The FEniCS Project version 1.5. *Arch. Numer. Softw.* **3**, 9–23.
70. Fgaier H, Eberl HJ. 2010 A competition model between *Pseudomonas fluorescens* and pathogens via iron chelation. *J. Theor. Biol.* **263**, 566–578. (doi:10.1016/j.jtbi.2009.12.003)